Polarization-independent tunable optical filters using bilayer polarization gratings

Elena Nicolescu and Michael J. Escuti*

Department of Electrical and Computer Engineering, North Carolina State University,
2410 Campus Shore Drive, Raleigh, North Carolina 27606, USA
*Corresponding author: mjescuti@ncsu.edu

We demonstrate a polarization-independent tunable optical filter based on switchable polarization gratings (PGs) formed using reactive and nonreactive liquid crystals (LCs). PGs are anisotropic diffraction gratings that exhibit unique properties, including a zero-order transmittance that is independent of incident polarization and that can vary from ∼0% to ∼100%, depending on wavelength and applied voltage. A stack of several PGs of varying thicknesses combined with an elemental angle filter yields polarization-independent bandpass tuning with minimal loss. We introduce a novel hybrid PG consisting of both reactive and nonreactive LC layers, which allows very thick gratings to be created with thin active LC layers. We demonstrate a tunable optical filter with a peak transmittance of 84% of unpolarized light, a minimum full width at half-maximum of 64 nm, and a maximum tuning range of 140 nm. © 2010 Optical Society of America

OCIS codes: 120.2440, 230.3720, 230.0250.

Tunable optical filters have a wide range of applications, including spectroscopy, optical communication networks, remote sensing, and biomedical imaging and diagnostics [1–3]. In recent years, research efforts have focused on miniaturizing tunable optical filters into physically small packages for compact portable spectroscopy and hyperspectral imaging applications, such as real-time medical diagnostics and defense applications [4]. Competing filter implementations, including dispersive elements matched with aperture stops (Czerny–Turner) [5,6], mechanically tuned etalons (Fabry–Perot) [7,8], liquid crystal (LC) tunable reflection filters [9,10], and assemblies of stacked birefringent wave plates and polarizers (Lyot, Solc, and Evans), [11,12] are not completely ideal for these applications due to the high cost of implementation, high insertion losses, strong polarization sensitivity, or difficulty in miniaturization.

Here we introduce an alternative tunable filter approach that is based on polarization gratings (PGs) [13–16], with the key advantage of having higher throughput and no polarizers. Also called anisotropic or vectorial gratings, PGs are a class of thin film diffractive elements, which are described as spatially varying, periodic profiles of optical anisotropy. They operate by periodically modulating the polarization state of the wavefront passing through them (as opposed to modulating phase or amplitude alone). These gratings can be created in two varieties: switchable [17,18] (tunable by applied voltage) and nonswitchable [19] (polymer). Both types of gratings exhibit the unique diffraction properties shown in Fig. 1(a).

For the purposes of this discussion, we will mainly be concerned with the zeroth diffracted order, which corresponds to the light that is directly transmitted through the grating having a diffraction angle $\theta_m = 0$. The zeroth-order diffraction efficiency (η_0) spectrum for light normally incident (within $\pm 20°$) is expressed as

$$\eta_0(\lambda) = \cos^2(\Gamma/2), \qquad (1)$$

where $\Gamma = 2\pi \Delta n d/\lambda$ is the retardation, Δn is the LC birefringence, d is the LC thickness, and λ is the
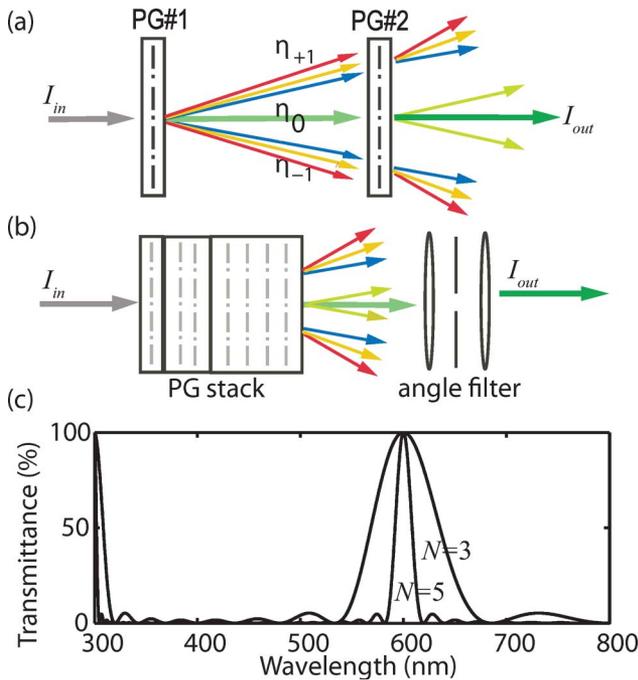
Fig. 1. (Color online) Stacked PG tunable optical filter concept. (a) Diffraction behavior of two stacked PGs. (b) General filter structure with PG stack and angle filter. (c) Representative transmittance spectra for filters with three and five stages, where each stage has twice the retardation of the previous, the peak wavelength is 600 nm, and the birefringence $\Delta n = 0.2$.

vacuum wavelength of incident light. Note that diffraction efficiency is a normalized term that describes the inherent diffraction behavior of a single PG, ignoring all absorption/reflection losses in the substrates or at the interfaces. Light that does not go into the zero order can diffract into only the $\pm$ first orders ($m = \pm 1$) with the diffraction angle (θ_m) governed by the grating equation, $\sin \theta_m = m\lambda/\Lambda + \sin \theta_{\text{in}}$.

Our filter concept comprises a stack of multiple PGs, as shown in Fig. 1, where the individual stages in the filter stack are PGs of increasing thickness. As light passes through the first grating, it diffracts such that the zero order contains a wide passband centered on the design wavelength, and all other wavelengths are coupled into the first orders. Light from the zero order then enters the second grating, and it diffracts again, resulting in a narrower passband coupled into the zero order [Fig. 1(a)]. Each additional grating is thicker than the previous and diffracts more wavelengths off axis, thereby achieving increasingly narrower passbands [Fig. 1(b)]. All but the zero order is then blocked using an angle filter. Note that in order to achieve proper separation of the orders, we stack the PGs such that the grating vector of each is rotated with respect to the previous. This results in the first orders being separated spatially, such that at the plane of the angle filter, the first-order diffracted beams are arranged in a circle around the zero order.

The transmittance of the system is a multiplication of each PG zero-order diffraction efficiency and the losses due to absorption/reflection from substrates and interfaces:

$$T(\lambda) = K^N \prod_{n=1}^{N} \eta_{0,n}(\lambda) = K^N \prod_{n=1}^{N} \cos^2\left(\frac{\pi \Delta n d_n}{\lambda}\right), \quad (2)$$

where N is the total number of stages, K is the transmittance of the substrates used in each individual PG element (essentially including any reflection and absorption of the electrodes), $\eta_{0,n}(\lambda)$ is the zeroth order diffraction efficiency of stage n, and d_n is the LC layer thickness of grating n. Note that the transmittance in Eq. (2) is a real-world measure of throughput, defined as the output intensity of the zero order (I_{out}) divided by the input intensity to the system (I_{in}). Figure 1(c) shows the representative transmittance spectra for ideal filters with three and five stages centered at 600 nm with birefringence $\Delta n = 0.2$ ignoring absorption and reflection losses.

The filter is tuned across the visible range by reducing its effective birefringence [$\Delta n(V)$] through applied voltage. By individually controlling each PG with an applied voltage, we lower the effective birefringence, shifting the passband toward lower wavelengths, according to Eq. (1). Depending on small fabrication variations, some of the PGs may be initially biased, so that the operational peak occurs at the design wavelength.

We identify three design possibilities or filter progressions involving the choice of d_n and N. Within each design, trade-offs between minimum possible full width at half-maximum (FWHM), minimum number of gratings, and maximum required grating thickness must be considered. The three progressions are exponential ($d = d_0 2^{n-1}$), linear ($d = d_0 n$), and compound (first three gratings follow the linear progression, then the third grating is repeated). Figure 2 shows simulation results for the three configurations, where $\Delta n = 0.2$, the thickness of the first grating is $d_0 = 3 \, \mu\text{m}$, and the design wavelength is $\lambda_0 = 600$ nm [20]. The simulation shows that the exponential progression is the optimum configuration for minimizing both FWHM and the number of gratings required. Minimizing the number of gratings is important because the minimal absorption of light by the indium tin oxide (ITO) and glass surfaces can become appreciable when multiplied through many interfaces. For example, a filter with target FWHM of 30 nm requires four, six, and thirteen gratings for the exponential, linear, and compound constructions, respectively.

The trade-off is that the exponential progression requires cells with a much thicker LC layer. For the same case as above, the exponential, linear, and compound progressions require a maximum LC layer thickness of $25 \, \mu\text{m}$, $15 \, \mu\text{m}$, and $9 \, \mu\text{m}$, respectively. As with all LC devices, large thicknesses (e.g., $d > 50 \, \mu\text{m}$) are not desirable because they tend to
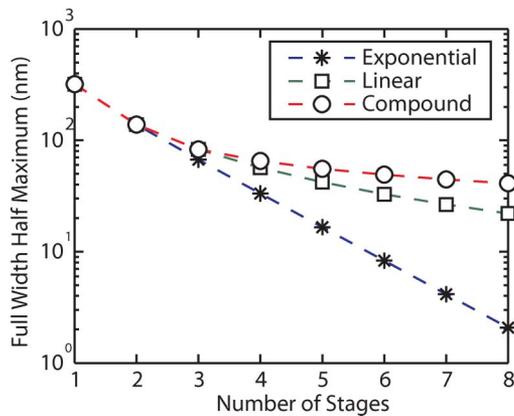
Fig. 2. (Color online) Theoretical plot of the relationship between the total number of PGs in the filter stack and the minimum FWHM achieved for the three filter configurations, where the peak wavelength is 600 nm, $\Delta n = 0.2$, and $d_0 = 3\,\mu m$.

have slow response times and are prone to defects. Furthermore, a larger thickness imposes a larger grating period (typically $\Lambda \geq 1.5d$) [21]. While this is achievable using holographic techniques, a large Λ leads to a small angle separating the zero and first orders and restricts the angular aperture of the tunable filter.

We overcome these limitations by introducing a novel bilayer PG (BPG) consisting of both reactive and nonreactive LC layers that allows very thick gratings to be created with thin active LC layers. The BPG is a combination of a switchable PG and a polymer PG with the basic structure shown in Figs. 3(a) and 3(b), where the polymer layer determines the nominal thickness of the grating and we add only a thin layer (one full-wave retardation) of nematic LC to achieve tuning by the applied voltage. This structure demonstrates two complex anchoring conditions with high quality: (i) a polymer PG aligning a switchable LC and (ii) a degenerate-planar anchoring surface with low pretilt enabling uniform orientation, without defects, of the switchable LC. The BPG exhibits the same favorable characteristics as a normal PG and can be directly integrated with the filter design described above.

The basic fabrication process of a BPG consists of a combination of the switchable and polymer PG fabrication steps [13,18]. First, a polarization hologram is created by superimposing two coherent orthogonally polarized beams from an ultraviolet laser with a small angle between them. Next, one ITO-coated glass substrate is coated with a photoalignment material, in this case, ROP103-2CP (Rolic Technologies, Limited). The substrate is then exposed to the polarization hologram, capturing the pattern in the photoalignment layer. The polymer LC RMS03-001C (Merck) is then spin coated onto the substrate in thin layers. After each layer is applied, it must be photopolymerized by exposure to UV light. This process is repeated until a polymer layer of the desired thickness is achieved. A second ITO glass substrate is then coated to achieve a degenerate-planar anchor-
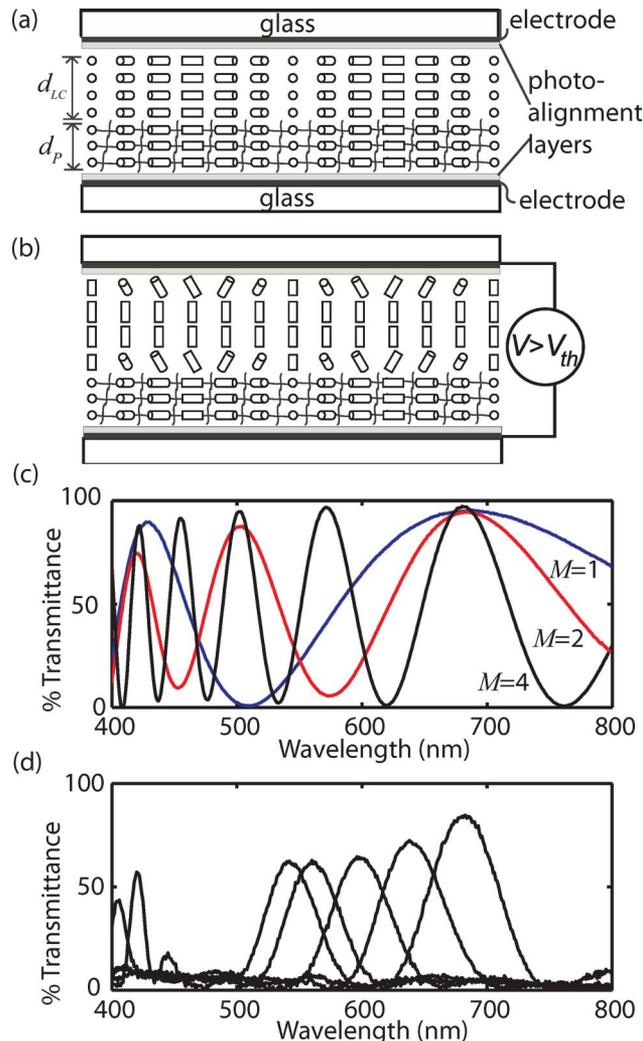

Fig. 3. (Color online) Structure of the BPG and experimental results of the BPG tunable optical filter. (a) BPG with no applied voltage, (b) BPG with applied voltage ($V \gg V_{\text{th}}$), (c) experimental spectra of three individual BPGs of exponentially increasing thickness, and (d) tuning characteristic of the entire three-stage BPG filter.

ing condition [22,23], which improves switchable LC alignment to the polymer surface. The two ITO substrates are then laminated together, such that a uniform thickness (usually a few μm) is achieved. Finally, a nematic LC (in this case MDA06-177, Merck) is injected into the cell gap and fills by capillary action. The surfaces direct the LC orientation to create the appropriate structure.

The diffraction from the BPG follows the same pattern as that of a traditional PG. Accounting for the individual retardation of each layer, the total retardation (Γ) is written as

$$\Gamma = 2\pi(\Delta n_p d_p + \Delta n_{\text{LC}} d_{\text{LC}})/\lambda, \qquad (3)$$

where d_P and Δn_P refer to the properties of the polymer layer and d_{LC} and Δn_{LC} refer to the properties of the switchable layer. The BPG has zero-order diffraction efficiency peaks occurring at wavelengths

$$\lambda_M = \Delta n_p d_p / M + \Delta n_{\mathrm{LC}} d_{\mathrm{LC}} / M, \qquad (4)$$

where M corresponds to the spectral fringe. The minimum value of the desired tuning range is set by the birefringence and thickness of the polymer layer, and the maximum limit of the tuning range is determined by the birefringence and thickness of the LC layer.

For experimental demonstration of our design, we built an exponential progression filter with three stages and a peak wavelength of 685 nm. The three gratings exhibited one, two, and four full waves of retardation at the center wavelength. The first grating had no polymer layer, and its LC layer was $4.8\,\mu\mathrm{m}$ thick. The second and third gratings had polymer layers of 4.6 and $9.1\,\mu\mathrm{m}$, respectively, in addition to the $4.8\,\mu\mathrm{m}$ LC layer. The thicknesses were calculated based on transmission spectra of the samples and material birefringence [24]. The three gratings were laminated together using the optical adhesive NOA65 (Norland Products).

We designed the PGs to have a grating period $\Lambda = 16\,\mu\mathrm{m}$, which leads to a diffraction angle $\theta_m = 2.3°$. We chose the grating period based on elastic-continuum theory [21], which suggests that the minimum grating period likely to support a defect-free structure for this design is $\geq 12\,\mu\mathrm{m}$.

In order to achieve proper angular filtering of the zero and first orders, we implemented a simple spatial filter [lens/stop/lens in Fig. 1(b)]. For this setup, we define two constraints on the divergence (Ω) of the input light:

$$\Omega \leq \arcsin(\lambda_{\min}/2\Lambda), \qquad (5\mathrm{a})$$

$$\Omega \leq \pi/N, \qquad (5\mathrm{b})$$

where Ω is the half-angle of the cone of the input beam, $\lambda_{\min}$ is the minimum wavelength in the spectrum that is within the tuning range of the filter, Λ is the grating period, and N is the number of stages in the filter. The first constraint ensures that there is no overlap between the zero order and the first orders. This equation comes from a direction cosine space analysis of PGs [25]. The second constraint ensures that there is no overlap between the first orders (achieved by rotating each grating vector), which could cause coupling of light back into the zero order. For any N, the maximum value of Ω is the smaller of the two values found in Eq. (5). In this experiment we used a collimated input and angular aperture of $\leq 2.3°$ for data collection.

Figure 3(c) shows the zero-voltage spectra of the three BPGs with $M = 1$, 2, and 4. Figure 3(d) shows the experimental spectrum of the filter as well as its tuning characteristics. The behavior of the filter is similar to the theoretical prediction, with a FWHM of $\sim 64\,\mathrm{nm}$ and a peak transmittance of $\sim 84\%$. Although the theoretical diffraction efficiency of each BPG is $\sim 100\%$, in the experimental result we see the effects of absorption and reflections within the sub-

Table 1. Results for Three-Stage BPG Tunable Optical Filter with Unpolarized Input Light

Voltage (V)	0	7	10	24	50
T_{peak} (%)	84	72	64	62	62
λ_{peak} (nm)	682	638	598	560	542
FWHM (nm)	64	59	53	49	47

strates and at interfaces as well as defects caused by nonideal fabrication techniques.

The filter shows low leakage in the stop bands. We also note the secondary spectral peak occurs at $\sim 420\,\mathrm{nm}$. This peak is used to measure the free spectral range (FSR), which refers to the distance between adjacent bandpass peaks. In this case, the FSR is $\sim 260\,\mathrm{nm}$—leading to a finesse of approximately 4.

The tuning range is approximately 140 nm, which is achieved by applying voltage across each of the BPGs, such that the grating is erased in the switchable LC portion of each cell, as in Fig. 3(b). The tuning range can be increased by increasing the thickness of the switchable LC layer. Table 1 shows how the transmittance, peak wavelength, and FWHM of the filter change with applied voltage. We notice a reduction in the peak transmittance with applied voltage, which we suspect is caused by a spatially nonuniform tilt profile of the LC director as a voltage is applied. If so, then this is not a fundamental limitation and could be improved by more careful fabrication. We believe that photoalignment materials and processing techniques that enable stronger anchoring strength will reduce this effect. We also notice a reduction in the FWHM of the filter with applied voltage, which we attribute to dispersion effects.

In summary, we have experimentally demonstrated a polarization-independent tunable optical filter with a maximum peak transmittance of 84% of unpolarized light, minimum FWHM = 64 nm, a maximum tuning range of 140 nm, FSR = 260 nm, finesse = 4, and an initial peak wavelength of 685 nm. We also introduced a novel BPG with high quality that integrates both switchable and polymer varieties. We demonstrated a polarizer-free approach using materials and construction with strong potential for low cost and small size implementations. We also described the theoretical operation and discussed the design trade-offs. We have shown experimentally that the exponential progression is most favorable as long as the switchable layer remains thin (i.e., by implementing the BPG). In order to further improve on current results, we suggest the addition of more stages to the filter in the exponential progression.

References

1. S. Woltman, G. Jay, and G. Crawford, "Liquid-crystal materials find a new order in biomedical applications," Nat. Mater. **6**, 929–938 (2007).

2. N. Gat, "Imaging spectroscopy using tunable filters: a review," Proc. SPIE **4056**, 50–64 (2000).

3. G. Keiser, "A review of WDM technology and applications," Opt. Fiber Technol. **5**, 3–39 (1999).

4. C. Bacon, Y. Mattley, and R. DeFrece, "Miniature spectroscopic instrumentation: applications to biology and chemistry," Rev. Sci. Instrum. **75**, 1–16 (2004).

5. K. Rosfjord, R. Villalaz, and T. Gaylord, "Constant-bandwidth scanning of the Czerny–Turner monochromator," Appl. Opt. **39**, 568–572 (2000).

6. A. Kenda, W. Scherf, R. Hauser, H. Gruger, and H. Schenk, "A compact spectrometer based on a micromachined torsional mirror device," in *Proceedings of IEEE Sensors, 2004* (IEEE, 2004), pp. 1312–1315.

7. A. Kutyrev, C. Bennett, S. Moseley, D. Rapchun, and K. Stewart, "Near infrared cryogenic tunable solid Fabry–Perot spectrometer," Proc. SPIE **5492**, 1172–1178 (2004).

8. K. Hirabayashi, H. Tsuda, and T. Kurokawa, "Tunable liquid-crystal Fabry–Perot interferometer filter for wavelength-division multiplexing communication systems," J. Lightwave Technol. **11**, 2033–2043 (1993).

9. H. Xianyu, S. Faris, and G. Crawford, "In-plane switching of cholesteric liquid crystals for visible and near-infrared applications," Appl. Opt. **43**, 5006–5015 (2004).

10. J. McMurdy, G. Crawford, and G. Jay, "Ferroelectric liquid crystal based tunable microspectrometer," Mol. Cryst. Liq. Cryst. **476**, 61–76 (2007).

11. O. Aharon and I. Abdulhalim, "Tunable optical filter having a large dynamic range," Opt. Lett. **34**, 2114–2116 (2009).

12. H. Morris, C. Hoyt, P. Miller, and P. Treado, "Liquid crystal tunable filter Raman chemical imaging," Appl. Spectrosc. **50**, 805–811 (1996).

13. L. Nikolova and T. Todorov, "Diffraction efficiency and selectivity of polarization holographic recording," J. Mod. Opt. **31**, 579–588 (1984).

14. C. Oh and M. Escuti, "Numerical analysis of polarization gratings using the finite-difference time-domain method," Phys. Rev. A **76**, 043815 (2007).

15. C. Provenzano, P. Pagliusi, and G. Cipparrone, "Highly efficient liquid crystal based diffraction grating induced by polarization holograms at the aligning surfaces," Appl. Phys. Lett. **89**, 121105 (2006).

16. S. R. Nersisyan, N. V. Tabiryan, D. M. Steeves, and B. R. Kimball, "Optical axis gratings in liquid crystals and their use for polarization insensitive optical switching," J. Nonlinear Opt. Phys. Mater. **18**, 1–47 (2009).

17. M. Escuti and W. Jones, "Polarization-independent switching with high contrast from a liquid crystal polarization grating," SID Symposium Digest **37**, 1443–1446 (2006).

18. J. Eakin, Y. Xie, R. Pelcovits, M. Radcliffe, and G. Crawford, "Zero voltage Freedericksz transition in periodically aligned liquid crystals," Appl. Phys. Lett. **85**, 1671–1673 (2004).

19. M. Escuti, C. Oh, C. Sánchez, C. Bastiaansen, and D. Broer, "Simplified spectropolarimetry using reactive mesogen polarization gratings," Proc. SPIE **6302**, 630207 (2006).

20. E. Nicolescu and M. Escuti, "Polarization-independent tunable optical filters based on liquid crystal polarization gratings," Proc. SPIE **6654**, 665405 (2007).

21. R. Komanduri and M. Escuti, "Elastic continuum analysis of the liquid crystal polarization grating," Phys. Rev. E **76**, 021701 (2007).

22. I. Dozov, D. Stoenescu, S. Lamarque-Forget, P. Martinot-Lagarde, and E. Polossat, "Planar degenerated anchoring of liquid crystals obtained by surface memory passivation," Appl. Phys. Lett. **77**, 4124–4126 (2000).

23. R. Komanduri and M. Escuti, "High efficiency reflective liquid crystal polarization gratings," Appl. Phys. Lett. **95**, 091106 (2009).

24. M. Escuti, D. Cairns, and G. Crawford, "Optical-strain characteristics of anisotropic polymer films fabricated from a liquid crystal diacrylate," J. Appl. Phys. **95**, 2386–2390 (2004).

25. C. Oh, J. Kim, J. Muth, and M. Escuti, "A new beam steering concept: Risley gratings," Proc. SPIE **7466**, 746619 (2009).